

Stability of metal-rich very massive stars

J. Goodman[★] and Christopher J. White

Princeton University Observatory, 4 Ivy Lane, Princeton, NJ 08544, USA

Accepted 2015 November 16. Received 2015 November 2; in original form 2015 March 3

ABSTRACT

We revisit the stability of very massive non-rotating main-sequence stars at solar metallicity, with the goal of understanding whether radial pulsations set a physical upper limit to stellar mass. Models of up to 938 solar masses are constructed with the MESA code, and their linear stability in the fundamental mode, assumed to be the most dangerous, is analysed with a fully non-adiabatic method. Models above $100 M_{\odot}$ have extended tenuous atmospheres (‘shelves’) that affect the stability of the fundamental. Even when positive, this growth rate is small, in agreement with previous results. We argue that small growth rates lead to saturation at small amplitudes that are not dangerous to the star. A mechanism for saturation is demonstrated involving non-linear parametric coupling to short-wavelength g-modes and the damping of the latter by radiative diffusion. The shelves are subject to much more rapidly growing strange modes. This also agrees with previous results but is extended here to higher masses. The strange modes probably saturate via shocks rather than mode coupling but have very small amplitudes in the core, where almost all of the stellar mass resides. Although our stellar models are hydrostatic, the structure of their outer parts suggests that optically thick winds, driven by some combination of radiation pressure, transonic convection, and strange modes, are more likely than pulsation in the fundamental mode to limit the main-sequence lifetime.

Key words: asteroseismology – instabilities – stars: massive.

1 INTRODUCTION

The threshold of hydrogen burning ($\approx 0.08 M_{\odot}$) is generally accepted as a physical lower limit to the masses of stars, one that is independent of the environment in which stars form. Whether there is a definite upper limit to stellar masses, and to what extent the limit may depend on nature (stellar physics) or nurture (star-forming environment) are open questions. The highest well-measured dynamical masses are $\sim 80 M_{\odot}$ (Schnurr 2012), most notably the double-lined eclipsing binary WR 20a (Bonanos et al. 2004; Rauw et al. 2004). Statistics of stars in galactic open clusters have been interpreted as evidence for an upper limit $\sim 150 M_{\odot}$ (Weidner & Kroupa 2004; Figer 2005; Oey & Clarke 2005; Koen 2006), while Crowther et al. (2010) present spectroscopic arguments for larger masses among the stars in the cluster R136 of the Large Magellanic Cloud. An empirical mass limit, if such exists, may reflect the environment in which most stars are observed to form: that is to say, molecular clouds, where the density of hydrogen nuclei is typically $n \lesssim 10^3 \text{ cm}^{-3}$, the temperature $\lesssim 100 \text{ K}$, and dust is abundant.

One of us has previously argued that the broad-line regions of bright quasi-stellar object (QSO) accretion discs are likely self-gravitating and prone to form very massive stars – at least several

hundred solar masses at the onset of gravitational instability, and perhaps $\gtrsim 10^5 M_{\odot}$ after accretion up to the isolation mass (Goodman & Tan 2004; Jiang & Goodman 2011). A QSO disc at $\sim 10^3$ gravitational radii from the black hole is a very different environment from a molecular cloud: denser by many orders of magnitude, hotter than the sublimation temperature of dust, rapidly rotating and shearing, and dominated by radiation pressure rather than gas pressure. Hence a different initial mass function and maximum stellar mass might result in such discs than in giant molecular clouds. On the other hand, it is well known that very massive stars are fragile due to the predominance of radiation over gas pressure, radiatively driven winds, and pulsational instabilities. Thus it is possible that internal physics establishes an upper limit $\lesssim 10^2\text{--}10^3 M_{\odot}$. A presumably fatal relativistic instability sets in above $10^5\text{--}10^6 M_{\odot}$, depending upon internal rotation (Chandrasekhar 1964; Baumgarte & Shapiro 1999; Montero, Janka & Müller 2012, and references therein). This leaves a gap of several orders of magnitude above the largest observed masses, however.

In the present paper, we return to the question of pulsational instabilities driven by the κ - and ϵ -mechanisms, which are sensitive to composition via opacities and to nuclear reaction rates. This is a problem that has been considered by many authors since the original work by Schwarzschild & Härm (1959), and one might have thought it a closed subject. However, the understanding of the opacities and other microphysical inputs has evolved, while the effects of convection on the linear growth rates remain uncertain,

[★] E-mail: jeremy@astro.princeton.edu

as do the mechanisms responsible for non-linear saturation of the pulsations if they grow at all.

We focus on the fundamental radial mode, on the assumption that it is most dangerous. Glatzel & Kiriakidis (1993, hereafter **GK93**) have analysed the stability of solar metallicity stars up to $120 M_{\odot}$ and found a host of higher order modes that grow more quickly than the fundamental. However, the energies of these modes are concentrated in the outer parts of the star, so that they can be expected to reach non-linear amplitudes before the bulk of the mass is much affected. The fundamental involves the entire star. Its character and scaling with mass are unlike those of other modes. The pulsation period increases $\propto M^{1/2}$, whereas those of higher order radial modes scale $\propto M^{1/4}$. This is due to the predominance of radiation pressure, $P_{\text{rad}}/P_{\text{gas}} \propto M^{1/2}$ for $M \gtrsim 100 M_{\odot}$, which makes very massive non-rotating stars almost neutrally stable against changes in radius even in the adiabatic approximation. Thus at large amplitudes ($\delta r/r \gtrsim 1$), the fundamental mode might disrupt or collapse the entire star. The former requires unbinding the star which becomes less difficult with increasing mass because of the predominance of radiation pressure and the attendant near-cancellation of gravitational and potential energies in hydrostatic equilibrium. (Indeed, spontaneous disruptions occurred in the simulations of AGN disc fragmentation by Jiang & Goodman 2011, though they were caused by numerical energy errors rather than pulsations.) Collapse might occur under extreme compression due to electron–positron pairs at central temperatures approaching 10^9 K, or due to relativistic corrections to gravity at masses $> 10^4 M_{\odot}$ (Zeldovich & Novikov 1971).

Recently, Shiode, Quataert & Arras (2012, hereafter **SQA**) have revisited the ϵ -mechanism. Applying a quasi-adiabatic analysis to equilibrium models constructed with the MESA code (Paxton et al. 2011, 2013), they concluded that the instability is suppressed by the effective viscosity due to turbulent convection, at least for stars of masses $\lesssim 1000 M_{\odot}$. However, they did not consider any models above $100 M_{\odot}$ with solar or higher metallicity. Since QSO discs appear to be metal rich, with metallicities perhaps up to 10 times solar (Hamann & Ferland 1999; Dietrich et al. 2003; Matsuoka et al. 2011; Dhanda Batra & Baldwin 2014), one motivation for the present work was to repeat **SQA**'s analysis at higher metallicities and masses $> 10^2 M_{\odot}$. We also wanted to perform a fully non-adiabatic rather than quasi-adiabatic analysis. This is arguably less important for the ϵ -mechanism because it is driven deep within the star where the thermal time is very long. However, **SQA** also found evidence for instabilities driven by opacity variations in the envelope which they did not fully explore, perhaps because they had less confidence in the quasi-adiabatic approximation for those modes. Also, at least with modern opacities, the envelopes of high-mass stellar models at solar metallicity differ strikingly from those of corresponding Population III models, and this has interesting consequences for the mode structures.

Linear stability analysis is only a first step towards answering the question posed above. If instabilities are found, one must consider how they may saturate in order to decide whether they are likely to shorten the main-sequence lifetime. Early attempts to address the saturation of instabilities driven by the ϵ -mechanism gave conflicting results (Appenzeller 1970; Papaloizou 1973b), but little work has been done along these lines in recent decades. We will argue that even if the uncertain damping effects of convection are neglected, the linear growth rates are so small compared to the real part of the pulsation frequency that the pulsations will saturate by one or another weakly non-linear mechanism at small amplitudes that do not threaten the survival of these stars, at least

Table 1. Basic properties of our ZAMS models.

M/M_{\odot}	L/L_{\odot}	R/R_{\odot}	T_{eff} (K)	X_{c}
10.0	5.118×10^3	3.922	24 688	0.727
21.5	4.841×10^4	5.998	34 983	0.727
46.4	2.962×10^5	9.279	44 236	0.727
100	1.244×10^6	15.27	49 360	0.729
215	4.054×10^6	30.88	46 638	0.726
464	1.135×10^7	75.29	38 635	0.728
938	2.686×10^7	274.3	25 106	0.727

not before they have lived out most of the nominal minimum main-sequence lifetime ($\sim 3 \times 10^6$ yr). Instead, in view of the structure of our hydrostatic models, as well as a recent body of work on Wolf–Rayet and O-star winds, radiatively driven mass loss seems more likely than pulsational instabilities to limit the lifetimes of the most massive metal-rich stars. We hope to explore the scaling of the mass-loss time-scale (i.e. $|M/\dot{M}|$) with stellar mass in a future paper.

The outline of this paper is as follows. Section 2, supplemented by Appendix A, presents the equilibrium MESA models and our methods for the linear stability analysis. Section 3 highlights the extended atmosphere or ‘shelf’ seen in the higher mass models. Results for the growth rates and eigenfunction of the fundamental are given in Section 4, with particular emphasis on non-adiabatic effects in the shelf. **GK93**'s intrinsically non-adiabatic ‘strange modes’ are shown to extend to higher masses, where they have longer periods than the fundamental. Section 5 examines non-linear saturation of the fundamental through three-mode or parametric coupling to high-order non-radial g-modes, and (more briefly) saturation of strange modes in shocks. Since the stably stratified zones of our most massive models are relatively small, and would perhaps disappear entirely at some higher mass, the explicit estimates in Section 5 are intended to be illustrative of a larger class of weak non-linearities that will limit the amplitude of the fundamental when its growth rate is small. A summary of our conclusions and a discussion of future steps follows in Section 6.

2 METHOD

2.1 Equilibrium models and initial estimates

Like **SQA**, we generated zero-age main sequence (ZAMS) stellar models using the stellar evolution code MESA. Here we highlight the configuration settings used when they deviate from the defaults.

The initial mass is specified, with initial abundances $(X, Y, Z) = (0.73, 0.25, 0.02)$. The simulation begins in the pre-main-sequence phase at a large radius and low central temperature. The atmosphere is modelled as a ‘simple photosphere’. Convective mixing is implemented following Henyey, Vardya & Bodenheimer (1965) in regions determined to be convectively unstable by the Ledoux criterion.

The star is evolved until it is determined to lie on the main sequence, defined by the minimum photospheric radius. (MESA has its own way of deciding when the model has reached the main sequence, but we found its decisions unreliable for our higher mass models.) The nuclear and photospheric luminosities are then in equilibrium, and the central hydrogen abundance is only very slightly depleted. Table 1 lists some properties of the models, which are similar to those of **GK93** (within 5 per cent in L and 1 per cent in T_{eff}), except that theirs were limited to 40–120 M_{\odot} . The effective

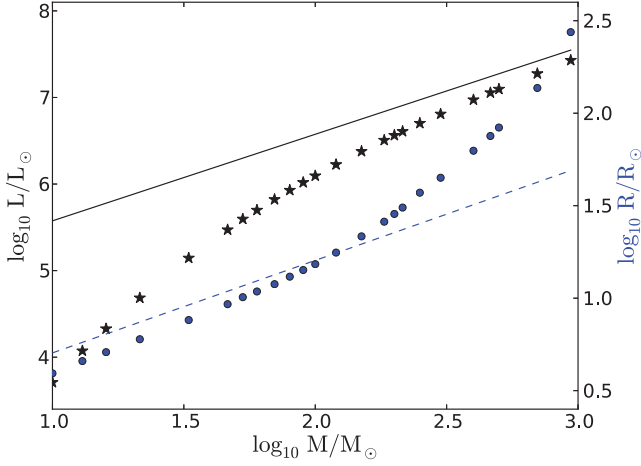


Figure 1. Luminosity (star symbols, left-hand scale) and photospheric radius (circles, right-hand scale) versus stellar mass for our MESA models. Thin solid line is the Eddington limit for this composition ($Y = 0.25$, $Z = 0.02$). Thin dashed line shows $R \propto M^{1/2}$, as would be expected for homologous radiation-pressure-dominated models.

temperature peaks at 4.95×10^4 K near $120 M_{\odot}$: more massive are cooler because of their distended atmospheric ‘shelves’ driven by iron opacities (Section 3). Luminosities and radii for additional models are shown in Fig. 1.

Once the star has reached its ZAMS phase, the model is saved and the data are analysed with the ADIPLS package (Christensen-Dalsgaard 2008), which computes adiabatic pulsational modes given one-dimensional stellar models. The output from ADIPLS is a set of eigenfrequencies and corresponding mode shapes in the form of radial displacements from equilibrium. We use these outputs in our own routine, which finds mode frequencies and shapes without the adiabatic assumption. We turn to this method now.

2.2 Non-adiabatic analysis

For the purpose of analysing the pulsational modes in a non-adiabatic framework, we began by adopting the method outlined in Castor (1971), with mass fraction as the independent variable, and a Henyey-type relaxation scheme for finding the eigenfrequencies. Despite extensive efforts and algorithmic variations, this did not give numerically stable results for the growth rate of the fundamental mode, possibly because of the many orders of magnitude separating the dynamical and thermal time-scales in the core, and the enormous radial variation in the ratio of these time-scales through the star.

We therefore adopted a sort of shooting method designed for very stiff equations (Appendix A). The basic linearized equations are

$$\frac{\partial}{\partial r} \delta P_{\text{gas}} = \rho \left[\omega^2 \delta r + g_{\text{rad}} \left(\frac{\delta \kappa}{\kappa} + \frac{\delta L_{\text{rad}}}{L_{\text{rad}}} \right) + 4g_{\text{eff}} \frac{\delta r}{r} \right], \quad (1a)$$

$$r^{-2} \frac{\partial}{\partial r} (r^2 \delta r) = -\frac{\delta \rho}{\rho}, \quad (1b)$$

$$\frac{\partial}{\partial r} \delta P_{\text{rad}} = -\rho g_{\text{rad}} \left(\frac{\delta \kappa}{\kappa} + \frac{\delta L_{\text{rad}}}{L_{\text{rad}}} - 4 \frac{\delta r}{r} \right), \quad (1c)$$

$$\frac{\partial}{\partial r} \delta L = i\omega 4\pi r^2 \rho T \delta S + 4\pi r^2 \rho \frac{\delta \epsilon}{\epsilon}. \quad (1d)$$

Here $g_{\text{rad}} = \kappa L_{\text{rad}} / 4\pi r^2 c$ is the radiative force per unit mass, $g_{\text{eff}} = GM_r / r^2 - g_{\text{rad}}$ is the residual between the gravitational and radiative accelerations, δ represents Lagrangian perturbation (first-order variation at fixed interior mass), and all other symbols have their usual meaning. We define dimensionless linearized variables

$$y_0 \equiv \frac{\delta r}{r}, \quad y_1 \equiv \frac{\delta \rho}{\rho}, \quad y_2 \equiv \frac{\delta T}{T}, \quad y_3 \equiv \frac{\delta L_{\text{rad}}}{L}. \quad (2)$$

Notice that L not L_{rad} appears in the denominator of y_3 .

In principle $\delta L = \delta L_{\text{rad}} + \delta L_{\text{conv}}$. However, since there is no generally accepted prescription for time-dependent convective luminosity – especially in the radiation-pressure-dominated regime – we adopt $\delta L_{\text{conv}} = 0$ (‘frozen convection’). Nor have we allowed for a turbulent convective viscosity in the linearized momentum equation (1a).

Then in terms of our dimensionless variables, with primes for d/dr and writing $f \equiv L_{\text{rad}}/L$, $\kappa_T = (\partial \ln \kappa / \partial \ln T)_{\rho}$, $\kappa_{\rho} = (\partial \ln \kappa / \partial \ln \rho)_{T}$, and similarly for ϵ_T and ϵ_{ρ} , equations (1) become

$$r y_0' = -3y_0 - y_1, \quad (3a)$$

$$y_1' + y_2' = \frac{\rho}{P_{\text{gas}}} [\omega^2 r y_0 + g_{\text{rad}} (\kappa_{\rho} y_1 + \kappa_T y_2 + f^{-1} y_3) + g_{\text{eff}} (4y_0 + y_1 + y_2)], \quad (3b)$$

$$y_2' = -\frac{\rho g_{\text{rad}}}{4P_{\text{rad}}} [\kappa_{\rho} y_1 + \kappa_T y_2 + f^{-1} y_3 - 4y_0 - 4y_2], \quad (3c)$$

$$r y_3' = \frac{4\pi r^3 \rho}{L} \{i\omega C_V T [y_2 - (\Gamma_3 - 1)y_1] + \epsilon (\epsilon_{\rho} y_1 + \epsilon_T y_2 - y_3)\}. \quad (3d)$$

The system of equations is closed by choosing four boundary conditions. Physically, one expects $\delta r = \delta L = \delta L_{\text{rad}} = 0$ at $r = 0$. This does not require y_0 or y_3 to vanish at the centre, but from the first of equations (3), one sees that non-singular behaviour requires

$$3y_0 + y_1 \rightarrow 0 \text{ as } r \rightarrow 0. \quad (4)$$

Similarly, regularity of the last of equations (3) implies

$$\frac{i\omega C_V T}{\epsilon} [y_2 - (\Gamma_3 - 1)y_1] + \epsilon_{\rho} y_1 + \epsilon_T y_2 - y_3 \rightarrow 0 \text{ as } r \rightarrow 0. \quad (5)$$

The factor in front of the square brackets is $\sim t_{\text{KH}}/t_{\text{dyn}} \gg 1$ if $\omega \sim t_{\text{dyn}}^{-1}$, so to a first approximation the behaviour near the origin is adiabatic, $\delta \ln T \approx (\Gamma_3 - 1)\delta \ln \rho$. But since we are interested in growth or decay rates $\omega_I \sim t_{\text{KH}}^{-1}$, we use equation (5) as written.

The outer heat equation requires a more general analysis than is given by Castor, as the equations in that work only hold under the assumption that radiation pressure is negligible compared to gas pressure at the outer boundary. This condition clearly does not hold for very massive stars. We therefore turn to the equation for radiation pressure in the Eddington approximation:

$$P_{\text{rad}} = \frac{F}{c} \left(\tau + \frac{2}{3} \right),$$

where F is the radiative flux and τ is the optical depth at the location being considered. In more familiar variables,

$$P_{\text{rad}} = \frac{L_{\text{rad}}}{4\pi r^2 c} \left(\frac{\kappa \Delta m}{4\pi r^2} + \frac{2}{3} \right), \quad (6)$$

where Δm is the mass exterior to the point being considered, if the density scale height is $\ll r$. Linearizing yields

$$\frac{\delta P_{\text{rad}}}{P_{\text{rad}}} = \frac{\delta L_{\text{rad}}}{L} - 4 \left(\frac{\tau + 1/3}{\tau + 2/3} \right) \frac{\delta r}{r} + \left(\frac{\tau}{\tau + 2/3} \right) \frac{\delta \kappa}{\kappa},$$

or in dimensionless variables,

$$-4 \left(\tau + \frac{1}{3} \right) y_0 + \tau \kappa_\rho y_1 + \tau \kappa_T y_2 + \left(\tau + \frac{2}{3} \right) (y_3 - 4y_2) = 0. \quad (7)$$

We replace L_{rad} with L here because in practice the model extends far enough into the tenuous atmosphere as to make the contribution of L_{conv} negligible.

The outer momentum equation is closed as follows. The total pressure at a point near the surface, under a mass Δm and at a radius r , is

$$P = \frac{\Delta m}{4\pi} \left(\frac{\ddot{r}}{r^2} + \frac{GM}{r^4} \right) + \frac{L}{6\pi c r^2}, \quad (8)$$

if the mass shell Δm is thin and effectively hydrostatic in its accelerated frame. The last term in equation (8) is the radiation pressure extrapolated to the outer surface of the shell, where $\tau = 0$. Subtracting equation (6) from equation (8) yields

$$P_{\text{gas}} = \frac{\Delta m}{4\pi} \left(\frac{\ddot{r}}{r^2} + \frac{GM}{r^4} - \frac{\kappa L_{\text{rad}}}{4\pi r^4 c} \right). \quad (9)$$

Perturbing this yields

$$\frac{\delta P_{\text{gas}}}{P_{\text{gas}}} = -\frac{\delta r}{r} \left(4 + \frac{\omega^2 r^3}{\beta GM} \right) - \frac{1 - \beta}{\beta} \left(\frac{\delta L}{L} + \frac{\delta \kappa}{\kappa} \right),$$

or equivalently,

$$\left(4 + \frac{\omega^2 R^3}{\beta GM} \right) y_0 + \frac{1 - \beta}{\beta} (y_3 + \kappa_\rho y_1 + \kappa_T y_2) - y_1 - y_2 = 0, \quad (10)$$

where β is defined in terms of the Eddington luminosity $L_{\text{Edd}} = 4\pi GMc/\kappa$ by $L = (1 - \beta)L_{\text{Edd}}$.

3 THE SHELF

When MESA evolves massive stars with non-negligible metallicity, it generically produces an extended envelope outside the polytropic core of the star, as shown in Fig. 2. This extremely diffuse region, which is incipient in the $46 M_\odot$ model but prominent in those above $100 M_\odot$, occupies a progressively larger fraction of the star's radius but a minute fraction of its mass ($\Delta M_{\text{shelf}} \approx 3 \times 10^{-6} M$ for the $938 M_\odot$ model). It is overwhelmingly dominated by radiation pressure, much more so than the stellar core. Because of its slowly radially varying temperature and density, we call this region the 'shelf', although the density profile is actually inverted in its outermost part (Fig. 2). The opacity in the shelf rises above the electron-scattering value. Since hydrostatic equilibrium limits the radiative part of the luminosity to the value that just balances gravity, $L_{\text{rad}} = 4\pi GM_* c/\kappa(\rho, T)$, and since the luminosity is near-Eddington, the balance of the luminosity (up to half, in our most massive model) is carried by inefficient convection that approaches the adiabatic sound speed, i.e. the sound speed based on total rather than gas pressure. A similar shelf has been observed in models of Wolf-Rayet stars and attributed to a bump in the iron opacity at temperatures $\sim 1-2 \times 10^5$ K (Gräfener, Owocki & Vink 2012, and references therein).

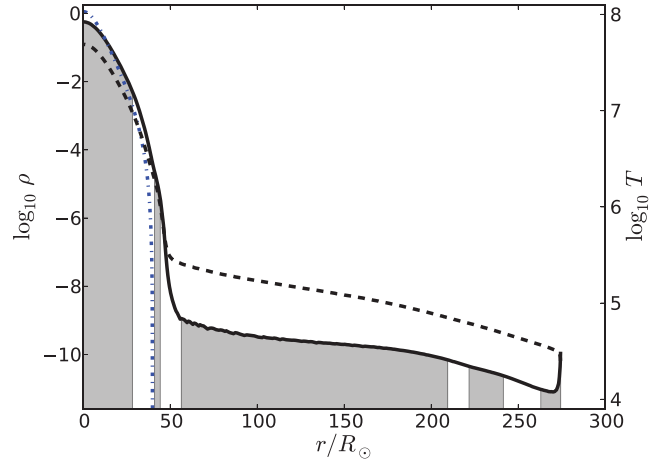


Figure 2. Density (solid line, left-hand ordinate) and temperature (dashed line, right-hand ordinate) in our $938 M_\odot$ model. Grey shading indicates convective regions. Dot-dashed line is the density profile of an $n = 3$ polytrope scaled according to equation (9) of Goodman & Tan (2004).

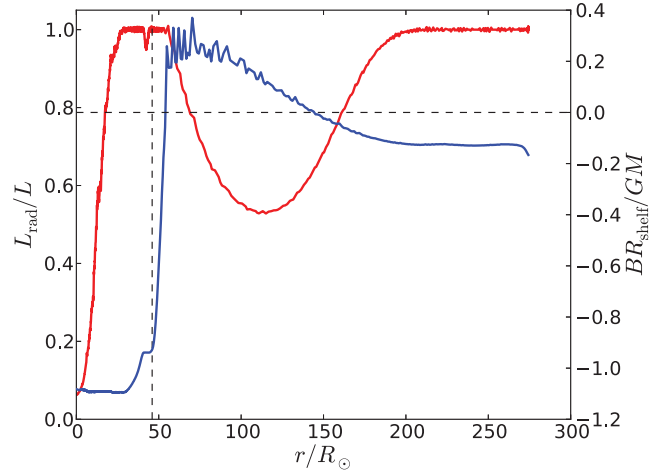


Figure 3. Left-hand axis, red curve: fraction of luminosity carried by radiative diffusion in the $938 M_\odot$ model. Right-hand axis, blue curve: Bernoulli 'constant' normalized by mass and radius at the base of the shelf.

MESA uses OPAL radiative opacities (Iglesias & Rogers 1996) in the density and temperature regime relevant to the shelf. We employ the so-called Type 1 opacities (carbon and oxygen abundances not determined independent of metallicity) with 'solar' relative abundances as defined by Grevesse & Noels (1993). See Paxton et al. (2011), section 4.3, for more details.

In fact, the shelf might be replaced by a radiatively driven wind if the constraint of hydrostatic equilibrium were relaxed. This is suggested by the fact that the Bernoulli 'constant'

$$B = u + \frac{1}{2}v^2 + \frac{P}{\rho} + \Phi \quad (11)$$

becomes positive in the lower part of the shelf (Fig. 3), though it changes sign once more in the outer convective regions. Here u is the internal energy per unit mass, and v is the mean radial velocity, which of course vanishes in these hydrostatic models, and $\Phi(r)$ is the gravitational potential, defined to vanish as $r \rightarrow \infty$. The kinetic energy of the convection would further increase B . These regions being strongly non-adiabatic, however, $B > 0$ does not guarantee a successful wind.

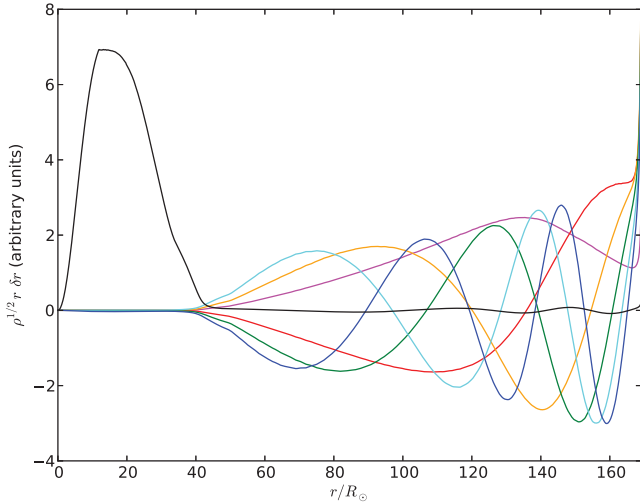


Figure 4. Plot of the lowest frequency adiabatic modes for the $464 M_{\odot}$ model. The curves show the square root of the mode kinetic energy per unit length, normalized independently. The modes have radial mode number n equal to 1 (red), 2 (orange), 3 (green), 4 (cyan), 5 (blue), 6 (magenta), or 7 (black), only the latter of which is not evanescent in the core.

For a precise definition of the base of the shelf, we use the radius or mass fraction corresponding to the local minimum in the pressure scale height, H_p . For the model shown in Fig. 2, this is $R_{\text{shelf}} = 46.3 R_{\odot}$. Within our suite of models, such a minimum occurs only for $M \gtrsim 50 M_{\odot}$.

4 RESULTS

4.1 Adiabatic calculations

First we describe the results obtained using ADIPLS. The seven lowest frequency modes for our $464 M_{\odot}$ model are shown in Fig. 4. Weighting the displacement δr by $\rho^{1/2} r$ shows where the energy of the mode is concentrated, in that ω^2 times the integral of the square of the plotted quantity gives the total energy.

Of particular note is that the first six modes discovered by ADIPLS are trapped in the shelf. The seventh mode is the true fundamental: its energy is concentrated in the core, where it has no nodes other than the centre, and it has an antinode at the base of the shelf (see Section 3). Some readers may object to our use of the term ‘fundamental’ for a mode that has multiple radial nodes. The adiabatic linearized problem is of Sturm–Liouville type, with orthogonal eigenfunctions having interleaved nodes. But the non-adiabatic problem is quite different. As Fig. 5 and Table 2 illustrate, the adiabatic and non-adiabatic versions of the fundamental (as we define it) are very similar – and both nodeless – in the core, and have nearly equal real parts of their eigenfrequencies, but can have different numbers of nodes in the shelf (11 and eight, respectively, for the real parts of the eigenfunctions shown in Fig. 5). Thus classification on the basis of numbers of nodes is not helpful in establishing a correspondence between the adiabatic and non-adiabatic eigenfunctions. Perhaps some other term such as ‘basic’ could be substituted for ‘fundamental’, but we feel that the latter is physically justified in this application.

ADIPLS also reports the frequencies of these modes, which are of course real in the adiabatic approximation. The corresponding periods, $2\pi/\omega$, of the fundamental modes differ only in the third or

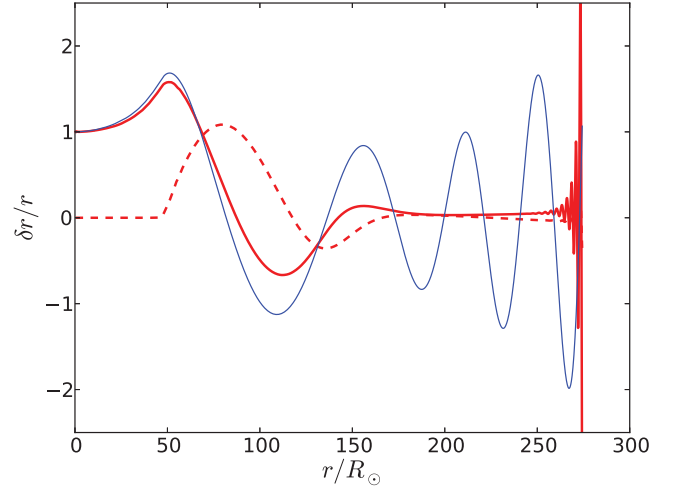


Figure 5. Fundamental radial mode at $938 M_{\odot}$. Thin blue line: adiabatic displacement eigenfunction. Red lines: real (solid) and imaginary (dashed) parts of the fully non-adiabatic displacement eigenfunction. Eigenfunctions are not multiplied by $r^2 \rho^{1/2}$, in order to emphasize behaviour in the shelf ($r > 46 R_{\odot}$).

Table 2. Periods and growth rates of fundamental radial mode. Negative growth rates indicate stability. Note $1 \text{ Md} \equiv 10^6 \text{ d}$.

M (M_{\odot})	Period (d)	Growth rate (Md^{-1})				
		ϵ	κ	Total	Convec.	No shelf
10	0.0905	−22.4	41.0	41.1	41.1	–
21.5	0.1391	−6.94	−10.3	−9.64	−9.68	–
46.4	0.2172	−3.01	−7.93	−6.33	−6.50	–
100	0.3279	−3.12	−2.37	+0.44	0.015	−1.73
215	0.4947	−19.5	−5.15	+9.28	8.45	+1.22
464	0.7253	−5.49	−11.1	−5.92	−7.19	+3.26
938	1.0435	−9.87	−15.5	−10.6	−11.9	+3.69

fourth significant digit from the values shown in the second column of Table 2 for the fully non-adiabatic fundamental modes.

4.2 Non-adiabatic calculations

In the linear equations, non-adiabaticity arises from two primary mechanisms. The nuclear heating rate per unit mass, ϵ , is sensitive to density and even more so to temperature. The strongly positive value of the logarithmic temperature derivative ϵ_T (≈ 12 near the centre of the $938 M_{\odot}$ model) tends to add entropy during the compressive phase of the pulsation cycle when $\delta T > 0$, thus producing mechanical work. This is the classic ϵ -mechanism. The entropy of mass elements varies also by radiative diffusion. This occurs in the linear analysis even if the opacity is constant, due to perturbations in the temperature gradient, but instability by the κ -mechanism generally requires that $\kappa_T > 0$ in regions of the star where the local thermal time $t_{\text{th}} \equiv L^{-1} C_V H_p dM_r/dr$ is comparable to the pulsation period (e.g. Cox 1980). Convection may tend to stabilize pulsations by providing an effective viscosity, but as discussed by SQA and references therein, the viscous effect is thought to be suppressed when the convective turnover time is long compared to the pulsation period. It is also possible for convection to drive instability when it adjusts rapidly to the changing superadiabatic gradient (Brickhill 1991). Except for a quasi-adiabatic estimate along the lines of SQA,

we have generally neglected these convective effects, even though these stars are in fact largely convective.

When applying the numerics described in Section 2.2, we are free to set any of ϵ_T , ϵ_ρ , κ_T , and κ_ρ to zero throughout the model. In this way we can separate the two effects. Thus the third column of Table 2 lists the growth rates obtained when the derivatives of κ are neglected, and similarly the fourth column gives the rates when the derivatives of ϵ are set to zero, while the fifth column retains all derivatives.

The effects of the non-adiabatic mechanisms on the growth rate are not entirely additive, as they would be in the quasi-adiabatic approximation. This is because the opacity derivatives have a substantial effect on the shape of the eigenfunction near the photosphere (or in the shelf), which is also the region mainly responsible for driving or damping. However, the ϵ -mechanism does appear to be additive, as might be expected since it acts only in the core where the quasi-adiabatic approximation is excellent. That is to say, if $\omega_I^{(\epsilon)}$, $\omega_I^{(\kappa)}$, and ω_I represent the growth rates in the third through fifth columns of Table 2, while $\omega_I^{(0)}$ is the growth rate obtained when all of ϵ_T , ϵ_ρ , κ_T , κ_ρ are neglected (this is not shown in the table), then we do find that $\omega_I^{(\epsilon)} - \omega_I^{(0)} \approx \omega_I - \omega_I^{(\kappa)}$ for all of the models except perhaps the first ($10 M_\odot$), in which the ϵ -mechanism is very weak.

The sixth column in Table 2 differs from the fifth by including a quasi-adiabatic work-integral estimate of convective viscous damping, following equations (11) and (12) of SQA. Since the quasi-adiabatic method depends upon the adiabatic eigenfunction, and since the adiabatic and non-adiabatic eigenfunctions differ strongly in the shelf region, we truncate the work integrals at the local minimum in the pressure scale height.

It can be seen that the two most massive models are stable without the convective correction. This appears to be due to radiative damping in the shelf. In Fig. 5, the first two nodes of the real part of the displacement occur $r \approx 87$ and $141 R_\odot$, where the imaginary part is close to a local maximum and minimum, respectively. (Recall that the shelf begins at $46 R_\odot$.) Thus the phase increases with radius, as for an outward-propagating acoustic wave. Evidently this wave is damped almost completely, because if it were not, then upon reflection from the photosphere a standing wave would result with real and imaginary parts in phase. The escaping acoustic power can be estimated as $\dot{E}_{ac} = 2\pi r^2 \rho c_s |\delta v|^2$, where $\delta v = -i\omega \delta r$ is the radial velocity perturbation and $c_s \equiv (\Gamma_1 P/\rho)^{1/2}$ is the adiabatic sound speed. Evaluating this at the first node and dividing by twice the total mode energy, $2E_{mode} = 4\pi \int \rho r^2 |\delta v|^2 dr$, yields an estimate for the damping rate of the mode amplitude: 11 Md^{-1} . This agrees well with the directly calculated growth rate shown for this model in the fifth column of Table 2. Of course the calculations are not independent because the estimate above uses the non-adiabatic eigenfunction. But it does suggest that the non-adiabatic calculation is self-consistent, and also that acoustic radiation into the shelf is the dominant loss mechanism at our highest masses. As further evidence of this, the final column of Table 2 shows growth rates calculated when the ‘photospheric’ boundary conditions (7) and (10) are imposed at the local minimum of the pressure scale height (which does not exist in the two least massive models), thus effectively discarding the shelf region from the linear analysis. This results in a small positive growth rate.

4.3 Strange modes

In addition to the fundamental mode, there are in principle an infinite number of other radial modes. Some, like the fundamental itself, are

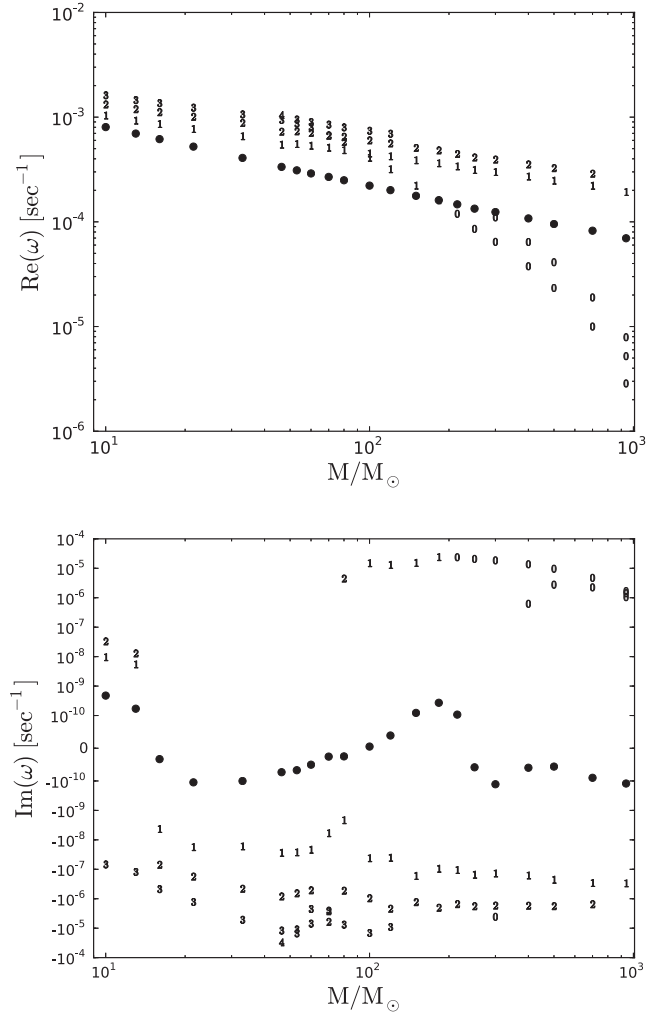


Figure 6. Real (first panel) and imaginary (second panel) parts of the lowest lying modes versus stellar mass. (Positive imaginary parts indicate instability.) Solid circles mark the fundamental. Other modes are marked by the number of nodes of $\delta r/r$ in the core. $M/M_\odot \in \{10, 13, 16, 21.5, 33, 46.4, 53, 60, 70, 80, 90, 100, 120, 150, 183, 200, 215, 250, 300, 400, 465, 500, 700, 983\}$.

slight modifications of adiabatic counterparts and are concentrated in the core (the region below the local minimum of the pressure scale height). The real parts of the frequencies of these increase with the number of nodes in the displacement eigenfunction ($\delta r/r$), while the imaginary parts tend to become more negative (i.e. more damped) but are generally small because of the long thermal time in the core.

Besides these, there are modes that have no obvious adiabatic counterpart, and which are probably the strange modes discussed by GK93 and Papanoizou et al. (1997). Though some of these are damped, others have positive growth rates [$\text{Im}(\omega) > 0$] whose reciprocals approach the dynamical time. Their energies are strongly concentrated in the tenuous shelf region and thus are not likely to affect directly the bulk of the star. This is discussed more quantitatively below (Section 5.2).

Fig. 6 shows the complex eigenfrequencies versus mass for the models in Table 1 and Fig. 6. For each mass, we show the four or five modes with smallest real part – at least among those we

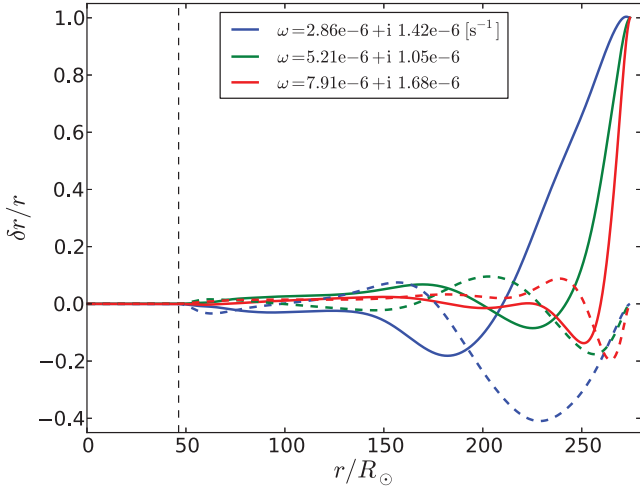


Figure 7. Three strange modes of the $938 M_{\odot}$ model, with frequencies as shown. Solid and dashed curves show real and imaginary parts of the eigenfunctions, respectively. Thin vertical dashed line divides the core from the shelf (see Fig. 2). Note eigenfunctions are not weighted by $r^2 \rho^{1/2}$.

have found.¹ Below approximately $50 M_{\odot}$, these are of the nearly adiabatic variety. At about $53 M_{\odot}$, however, the fourth and fifth harmonics cross: the real parts of their frequencies become nearly equal, and their eigenfunctions differ mainly in the nascent shelf region. By $60 M_{\odot}$, one of the pair – the one with smaller real part – has its energy almost wholly concentrated in the shelf. By $70 M_{\odot}$, the successor to this mode crosses the second harmonic; by $94 M_{\odot}$ it has crossed the first harmonic; and it crosses the fundamental at $183 M_{\odot}$. Up to about $70 M_{\odot}$, the strange modes are damped, but at $M \geq 80 M_{\odot}$ they grow vigorously (Fig. 6). Our most massive model has at least three strange modes with real parts of their eigenfrequencies below that of the fundamental, and growth times on the order of 10 d (Fig. 7). All but $\sim 10^{-8}$ of the energies of these three modes lie in the shelf.

Our identification of the rapidly growing shelf modes with the strange modes is based largely on the variation of their eigenfrequencies with mass and the concentration of their eigenfunctions in the shelf. Papaloizou et al. (1997) propose as the definitive test of ‘strangeness’ that the modes should persist in the limit that $\omega t_{\text{thermal}} \rightarrow 0$. We have not made this test but note that the shelf regions of our most massive models are even more extreme than those of GK93 with respect to radiation-pressure dominance and short thermal times. We refer the reader to Papaloizou et al. (1997) and GK93 for further discussion of the linear physics of strange modes.

5 NON-LINEAR SATURATION

Appenzeller (1970) proposed that radial pulsations of very massive stars saturate in shocks that eject mass. His criterion for the onset of shocks was that the radial velocity at the photosphere becomes larger than the local sound speed. Papaloizou (1973a) found

¹ It is possible that some low-lying modes have been missed. At the higher masses, the search for modes becomes tedious, especially for the strongly non-adiabatic modes. There are several causes, but the most pernicious is that each complex zero of the objective function described in Appendix A is paired with a pole, and the separation between poles and zeros decreases with increasing mass. This makes it difficult for zero-finders to ‘smell’ their quarry from a distance in the complex plane.

in his own numerical calculations that shocks were not so easily formed, and saturation occurred without mass loss. Our view is closer to Papaloizou’s, but we emphasize coupling to non-radial modes rather than radial overtones, at least for the fundamental and other near-adiabatic modes. Saturation of strange modes is more likely to yield shocks and is discussed briefly in Section 5.2 below.

The largest growth rates we find are $\lesssim 10 t_{\text{KH}}^{-1}$. Here t_{KH} is the Kelvin–Helmholtz time defined as by Goodman & Tan (2004), which asymptotes to $t_{\text{KH}} \approx 3000$ yr in the limit of very large masses.² On the other hand, the pulsation periods recorded in Table 2 are $\lesssim 1$ d, and we expect this to scale $\propto M^{-1/2}$ at higher masses. Thus the growth times are on the order of 10^5 pulsation periods. In this sense, the instabilities are extremely weak, even if the possibly stabilizing influence of convection is ignored.

At one level, this is not a surprise. Whether caused by the ϵ - or κ -mechanism, pulsational instability operates by modulating the heat content of the star on the pulsation period. Thus, the smallness of the ratio $|\omega_i/\omega_r|$ reflects the disparity between the characteristic thermal and dynamical times of the star. We shall shortly argue that the smallness of the linear growth rate implies a small amplitude at non-linear saturation.

This is not inconsistent with the relatively large amplitudes of oscillation of classical Cepheids ($\delta R/R \sim 0.1$) because the linear growth times are only ~ 100 pulsation periods in those stars (e.g. Castor 1971; Bono, Marconi & Stellingwerf 1999), and it is worth recalling why (e.g. Cox & Giuli 1968). Classical Cepheids are evolved stars with degenerate cores and a very large ratio of central to mean density. Consequently, the eigenfunction $\zeta(r) \equiv \delta r/r$ of the fundamental radial mode is very far from homologous, $\zeta(0)/\zeta(R) \sim \bar{\rho}/\rho(0) \ll 1$. The mode mass – the factor by which one multiplies the mean-square radial velocity at the surface to get the total energy in the mode – is many orders of magnitude smaller than the total mass of the star. In other words, for a given surface amplitude $\delta R/R$, the stored energy in the mode is much less than it would be if the pulsations were homologous, by a factor $\propto M_{\text{mode}}/M_*$. Since the driving regions for the κ -mechanism lie near the surface, the work integral is insensitive to the mode mass: it is of order $\Pi_0 \delta L \delta R/R$, where $\delta L/L \sim \delta R/R \sim -\delta T/T$ is the modulation of the surface luminosity and $\Pi_0 \equiv 2\pi\omega_r^{-1}$ is the pulsation period. Therefore the growth rate, which scales with the ratio of the work done per cycle to the stored energy in the mode, is $\sim (M_*/M_{\text{mode}}) t_{\text{KH}}^{-1}$. The ϵ -mechanism is negligible in Cepheids because the nuclear-burning regions are in shell sources near the centre, where $\delta \log T$ and $\delta r/r$ are much smaller than in the ionization zones.

As a quantitative example, we have used MESA to create a ‘Cepheid’ with the following parameters: $M_* = 5.7 M_{\odot}$, $R_* = 28.85 R_{\odot}$, $T_{\text{eff}} = 5900$ K, and $L = 906 L_{\odot}$. For this model, $\bar{\rho}/\rho(0) = 6.2 \times 10^{-8}$, while $\zeta(0)/\zeta(R_*) = 3.3 \times 10^{-6}$ and $M_{\text{mode}}/M_* = 8.4 \times 10^{-5}$ for the fundamental radial mode computed with ADIPLS. By contrast, for the $938 M_{\odot}$ main-sequence model we find $\zeta(0)/\zeta(R) = 0.66$ and $M_{\text{mode}}/M_* = 0.061$.³

² In order that the estimate of t_{KH} not be biased by the extended but almost massless shelf, we use for R the radius of the base of the shelf as defined in Section 3.

³ This depends upon what one considers to be the stellar ‘surface.’ For the purpose of calculating M_{mode} , we use R_{shelf} (Section 3) when this is distinctly less than the photospheric radius.

Thus the fundamental mode is approximately homologous and involves a significant fraction of the star's mass. We expect M_{mode}/M_* to be nearly constant and comparable to this for larger masses because of the similarity of these models to isentropic $n = 3$, $\Gamma_1 = 4/3$ polytropes. Thus we also expect the growth rates of the fundamental radial mode to remain $\lesssim 10\tau_{\text{KH}}^{-1}$, due to the relatively homogeneous structure and homologous pulsation of these very massive main-sequence models, regardless of the details of the excitation mechanisms and of the shelf or wind.

5.1 Saturation of the fundamental via three-mode coupling

As a general rule, instabilities with smaller linear growth rates saturate at lower amplitudes. A simple model equation for the amplitude envelope $A > 0$ might be

$$\frac{dA}{dt} = \omega_1 A - \nu A^{n+1}, \quad (12)$$

in which ω_1 is the linear growth rate, while ν and n describe the non-linearities. If ω_1 , ν , and n are all positive, then equilibrium is reached at $A_{\text{sat}} = (\omega_1/\nu)^{1/n}$. As noted above, pulsations in classical Cepheids grow relatively rapidly. Saturation in these stars and in RR Lyraes occurs via shocks and non-linear modification of the conditions in the driving (ionization) zones (Christy 1966). Because of their much smaller dimensionless growth rates ($\omega_i/\omega_r \sim 10^{-6}$ instead of $\sim 10^{-3}$), the massive main-sequence stars considered here may saturate at lower amplitudes, where more delicate non-linearities may be effective.

Dziembowski (1982) suggested that three-mode coupling is responsible for saturation in dwarf Cepheids, and that this explains why they oscillate at lower amplitudes than do classical Cepheids. He worked directly from non-linear equations of motion. But if dissipation is weak, an action principle, which is necessarily adiabatic, can be efficient in describing mode couplings. The Lagrangian density $\mathcal{L}(\xi, \dot{\xi})$ is expanded in powers of the displacement ξ and its time derivative $\dot{\xi}$. The quadratic terms (\mathcal{L}_2) yield the linearized equations of motion, while cubic and higher terms ($\mathcal{L}_3 + \mathcal{L}_4 + \dots$) describe non-linear couplings. When the amplitude of the primary/'parent' mode grows slowly from small amplitudes, the cubic non-linearities are the first to come into play. The most important couplings are those that are resonant, meaning that the linear eigenfrequencies of the parent and daughter modes satisfy $\omega_p \approx \omega_{d1} + \omega_{d2}$, so that secular transfers of energy can occur.⁴ However, the corresponding Hamiltonian density $\mathcal{H}_2 + \mathcal{H}_3$ cannot be positive definite since the components of ξ can have either sign, so that the higher order non-linearities must dominate if the amplitudes pass some threshold, perhaps leading to shocks and a breakdown of the Lagrangian description. Actually, even when the amplitudes remain small, dissipative terms must be added to the equations of motion to describe the linear damping of the daughter modes. In application to pulsating stars, the growth rate of the parent is also represented by a non-adiabatic term. The daughter modes are usually smaller in wavelength than the parent and therefore more easily damped by radiative diffusion or (perhaps) eddy viscosity.

Landmark applications of three-mode coupling to the saturation of stellar instabilities include those by Wu & Goldreich (2001) (to white dwarf/ZZ Ceti stars), as well as Schenk et al. (2002) and Arras et al. (2003) (to rapidly rotating neutron stars). Papaloizou

(1973a) argued that pulsations of very massive stars driven by the ϵ -mechanism can saturate via direct resonant couplings: that is, the coupling of a quadratic or higher power of the fundamental mode to a *higher* frequency radial p mode (overtone), so that $n\omega_f \approx \omega_d$ for some integer $n > 1$. Non-radial daughter modes offer many more possibilities for resonance, however, g-modes are necessarily non-radial and have low frequencies, which is important for resonances of the type $\omega_p \approx \omega_{d1} + \omega_{d2}$ because the frequency of the fundamental, ω_f , is somewhat lower relative to the characteristic dynamical frequency $\omega_* \equiv (GM_*/R_*^3)^{1/2}$ than in less massive stars, the ratio ω_f/ω_* scaling as $M^{-1/2}$ (Goodman & Tan 2004). Therefore we focus on couplings of this type. When the parent is the radial fundamental mode, the strongest three-mode couplings are usually parametric subharmonic, meaning that the two daughter modes are two copies of the same mode, with frequency $\omega_d \approx \omega_f/2$. The eigenfunction of a typical daughter mode is high order, with many nodes in radius and angle, but its square is non-negative and hence may have a significant three-mode coupling with the nodeless radial fundamental. Parametric subharmonic destabilization of g-modes and internal waves has been studied experimentally as well as theoretically (Benielli & Sommeria 1998, and references therein).

We use our most massive ($938 M_\odot$) model as an example. Most of the star convects, but there is a radiative zone at $29 \lesssim r/R_\odot \leq 41$ containing $0.026M$. (There is also a second radiative zone at $r \geq 44 R_\odot$, and still others in the shelf, but these contain much less mass, so we neglect them here.) The peak of the Brunt–Väisälä frequency is $N_{\text{max}} = 2.94\omega_*$, whereas the frequency of the fundamental radial mode is $\omega_f = 1.1446\omega_* \approx 7.116 \times 10^{-5} \text{ rad s}^{-1}$ according to ADIPLS (which computes only the real part), in good agreement with our non-adiabatic code. Thus there are many g-modes with frequencies $\sim \omega_f/2$. Using the approximate Wentzel–Kramers–Brillouin (WKB) dispersion for high-order g-modes,

$$\frac{\sqrt{l(l+1)}}{\omega_{ln}} \int N(r) \frac{dr}{r} \approx \pi \left(n - \frac{1}{2} \right) \quad (13)$$

(where $n \geq 1$ counts radial nodes) and the profile of the Brunt–Väisälä frequency in the radiative zone, $N(r)$, we estimate that $n/l \approx 0.34$ for $\omega_{ln} \approx \omega_f/2$ and $l, n \gg 1$. For a non-rotating spherical star, so that the eigenfrequency is independent of spherical-harmonic order m , the number of mode frequencies in a given interval $\Delta\omega$ near $\omega_f/2$ that correspond to g-modes of degree $l' \leq l$ scales as $0.17 l^2 \Delta \log \omega$ when $l \gg 1$. Inverting this, the minimum l at which one expects to find modes in the interval $\Delta\omega$ is

$$l_{\text{min}}(\Delta\omega) \approx 2.4 \left(\frac{\Delta\omega}{\omega} \right)^{-1/2}. \quad (14)$$

The distance $\Delta\omega$ from exact subharmonic resonance at which daughter modes can grow depends upon the linear damping rate of these modes, the amplitude of the parent, and the three-mode coupling coefficient. For the damping time of high-order g-modes by radiative diffusion, we apply equation (4.8) of Dziembowski (1982) to our $938 M_\odot$ model:

$$t_{\text{damp}} = \gamma_d^{-1} \approx 1.0 \left(\frac{30}{l} \frac{\omega_f}{2\omega} \right)^2 \text{ yr}. \quad (15)$$

We evaluate the three-mode coupling coefficient from equation (A8) of Kumar & Goldreich (1989). Their formula assumes that the adiabatic exponent Γ_1 is constant and neglects the Eulerian perturbation to the gravitational potential, which, although essential for the eigenfrequency of the fundamental mode, is unimportant for the coupling since most of the stellar mass lies interior to the

⁴ In resonance conditions such as this, all frequencies are understood to be real and non-negative.

propagation region of the g-modes in our case. We make the further approximation that the fundamental mode is exactly homologous, meaning that its radial displacement is given by $\delta r(r, t) = \zeta r \cos(\omega_f t)$, with ζ spatially constant but growing slowly as $\exp(\omega_i t)$. We approximate the daughter mode eigenfunctions using WKB, neglecting terms of relative order $(k_r H_p)^{-1}$, where $k_r \approx \sqrt{l(l+1)N/\omega r}$ is the radial wavenumber and H_p the pressure scale height, and find that

$$\int \mathcal{H}_3 d^3 \mathbf{x} = \dots + \left(\frac{3\Gamma_1 - 1}{2} \right) \zeta \cos \omega_f t \int N^2 \delta r_d^2 dM. \quad (16)$$

Here ‘...’ represents all three-mode coupling other than the one of interest, while $\delta r_d = q_d(t) \xi_{r,d}(r) Y_{lm}(\theta, \phi)$ is the radial displacement of the daughter mode, with time-dependent amplitude $q_d(t)$. For simplicity, we set $\Gamma_1 = 4/3$, though the mass-averaged value of Γ_1 in the 938 M_\odot model is ≈ 1.37 .

The integrand of equation (16) is twice the potential energy per unit mass of the g-mode. The coupling term can therefore be treated as though it were a time-dependent correction to the linear dynamics of the daughter mode, whose amplitude evolves according to

$$\ddot{q}_d + 2\gamma_d \dot{q}_d + \omega_d^2 [1 + 3\zeta \cos(\omega_f t)] q_d = 0. \quad (17)$$

As usual with such Mathieu equations, if ζ and γ_d/ω_d are both small, then the solutions for $q_d(t)$ are approximately sinusoidal but with envelopes varying as $\exp(st)$:

$$s = -\gamma_d \pm \frac{3\zeta \omega_d}{4} \sqrt{1 - \left(\frac{4\Delta\omega_d}{3\zeta \omega_d} \right)^2}, \quad \Delta\omega_d \equiv \omega_d - \frac{1}{2}\omega_f. \quad (18)$$

Thus in order that the daughter mode should grow even at exact resonance ($\Delta\omega_d = 0$), we must have $\zeta > 4\gamma_d/3\omega_d$. Since $\gamma_d \propto l^2$ (equation 15), this sets an upper bound to the degrees of daughter modes that can be destabilized when the amplitude of the fundamental is $\delta R/R = \zeta \ll 1$. Yet l must be large enough so that it is probable to find eigenfrequencies within the range $|\Delta\omega_d| \leq 3\zeta \omega_d/4$ for which the square root in equation (17) is real. Thus in effect we must evaluate γ_d at the degree l_{\min} that is found by setting $\Delta \log \omega \approx \zeta$ in equation (14). Then $\gamma_d \propto l_{\min}^2 \propto \zeta^{-1}$, so that the requirement $\frac{3}{4}\zeta \omega_d > \gamma_d$ for growth leads to an inequality of the form $\zeta > C\zeta^{-1}$. Evaluating the numerical factor C , we find that the threshold for exciting daughter modes is approximately

$$\left(\frac{\delta R}{R} \right)_{\min} \approx 3 \times 10^{-3}, \quad l_d \approx 45. \quad (19)$$

Since the mode frequencies are sensitive to details of the stellar model, the occurrence of resonance is effectively probabilistic, and therefore the threshold for subharmonic instability will vary somewhat. In fact, for the particular model considered here, ADIPLS finds $\Delta\omega_d/\omega_d \approx 4 \times 10^{-4}$ at $l_d = 26$, which is some 20 times closer to resonance than would be expected from the statistical estimate (14).

The threshold (19) of subharmonic instability involves only the current amplitude of the fundamental mode, not its rate of growth, ω_i . The latter is important for deciding whether the daughter modes can actually accept and dissipate energy from the parent faster than the non-adiabatic work integral increases that energy. Arras et al. (2003) state as a rule of thumb that the condition for this is simply $\gamma_d > \omega_i$, a regime they call ‘weak driving’. Clearly this would suffice for non-linear saturation of the unstable parent mode if a daughter mode could reach energy equipartition with the parent, but that is unlikely in our case. The wavelength of the first daughters to go unstable is much smaller than the radius of the star, roughly by a factor $2/l$ when one accounts for both the radial and angular components of the wavenumber. Also the mass of the g-mode propagation

zone is only $0.026M$, whereas the effective mass of the fundamental mode is $0.061M$, as previously discussed. Therefore if a daughter mode at, say, $l_d = 45$ were to have the same energy as the fundamental, it would have a strain rate (spatial derivative of velocity) roughly $2\pi(l/2)\sqrt{0.061/0.026} \approx 5.l$ times larger than the parent. At such a strain rate, the daughter mode would destabilize still other modes (granddaughters) and probably transfer energy to them more quickly than it could receive energy from the parent. Therefore equipartition is unlikely.

On the other hand, $\gamma_d \gg \omega_i$ in the present case, so that the rate of linear dissipation by daughter modes could balance the growth of the parent even if the daughters’ energies were well below equipartition with the parent. Because of the degeneracy of the eigenfrequencies in a non-rotating star, $2l_d + 1$ daughter modes grow at the same rate. When the average energy *per mode* reaches a value \bar{E}_d , the total linear dissipation rate becomes $2(2l_d + 1)\gamma_d \bar{E}_d$. Setting this equal to the rate at which the fundamental mode gains energy from its own linear instability, $2\omega_i E_f$, shows that saturation is possible when $\bar{E}_d/E_f \approx (2l_d + 1)^{-1}(\omega_i/\gamma_d)$. Evaluating this for $l_d = 45$, $\gamma_d^{-1} \approx 0.46 \text{ yr}$ (cf. equation 15), and $\omega_i = (500 \text{ yr})^{-1}$ leads to $\bar{E}_d/E_f \approx 10^{-5}$. The ratio of strain rates is then

$$\frac{1}{2} \sqrt{\frac{\bar{E}_d}{E_f}} 4.6 l_d \approx 0.3 \quad (l_d \approx 45) \quad (20)$$

(a factor of $1/2$ reflects the lower frequency of the daughters). Since this is less than unity, saturation of the parent/fundamental mode is likely at daughter amplitudes too small to excite granddaughters.

We conclude that it is indeed likely that three-mode coupling will saturate the growth of the fundamental radial mode. However, some caveats are in order regarding rotation, which we have so far neglected.

There are at least two rotational regimes to consider: slow and fast. Slow rotation at an angular velocity $\Omega \gtrsim l_d^{-1} \omega_*$ but $\ll N_{\max}$ will lift the degeneracy with respect to spherical-harmonic order m , while preserving the degree l as a useful approximate quantum number. Since there are more distinct eigenfrequencies, subharmonic resonance becomes possible at smaller l : equation (14) is replaced by $l_{\min} \approx 1.6(\Delta\omega/\omega)^{-1/3} \rightarrow 0.6\zeta^{-1/3}$. Otherwise following the same steps as before, the threshold of instability occurs at $\zeta \approx 5.4 \times 10^{-4}$ and $l_d \approx 20$ (both lower than before). Now a single, non-degenerate daughter mode first goes unstable, so the required balance at saturation if this daughter only is active becomes $2\gamma_d \bar{E}_d = 2\omega_i E_f$, and the ratio of strain rates (daughter:parent) works out to ≈ 3 instead of 0.3. Hence non-linear coupling of the daughter to granddaughters may occur, limiting the energy of the former and complicating the analysis. On the other hand, the number of unstable daughters will increase rapidly ($\propto \zeta^{5/2}$) as the amplitude of the parent increases above the first subharmonic threshold, so without having analysed the situation carefully, we still expect saturation to occur.

By fast rotation, we mean fast enough so that inertial oscillations – approximately incompressible motions restored by Coriolis rather than buoyancy forces – can have resonant three-mode couplings with the parent, as considered by Schenk et al. (2002) and Arras et al. (2003) for neutron stars. Since the maximum frequency of inertial oscillations is 2Ω , a necessary condition for subharmonic instability of the fundamental mode is $\Omega > \omega_f/4$. In the 938 M_\odot model, this translates to $\Omega > 0.286\omega_*$, which is half or less of the mass-shedding limit for an $n = 3$ polytrope, depending how one defines ω_* for a non-spherical body (Hurley & Roberts 1964). Rapid rotation is not unreasonable for a body recently formed by

fragmentation of an active galactic nucleus (AGN) accretion disc. Furthermore, ω_f/ω_* scales as $M^{-1/2}$ with increasing stellar mass.⁵ Unlike g-modes, inertial oscillations propagate in convection zones, so that they may be destabilized throughout these (largely convective) massive stars. This is salient because we are not sure how the mass fraction of the radiative zones should scale at masses above $10^3 M_\odot$ and supersolar metallicities. Even when the condition $\Omega > \omega_f/4$ is not satisfied, the imposition of rotation on vigorous convection will surely lead to magnetic fields, perhaps in rough equipartition with the convection, so that radial pulsations may couple non-linearly to small-scale Alfvénic modes.

5.2 Saturation of strange modes

Because of their large growth rates, strange modes are unlikely to saturate via three-mode couplings of the sort discussed above. They will grow to large amplitudes and probably saturate via shocks.

As a conservative criterion for the amplitude at which a shock appears, we take $|\partial\delta r/\partial r|_{\max} \geq 1$, since this would predict shell crossing in the absence of shocks. For the fastest growing strange mode of the 938 M_\odot model, $|\partial\delta r/\partial r|_{\max} = 25.9\delta R/R$. The maximum is achieved at $r = 0.984R$. Shocks may then appear when the surface amplitude $\delta R/R = (25.9)^{-1} \approx 4$ per cent. At this point, the amplitude of the displacement eigenfunction at the surface of the core ($r \approx 0.169R$) will be only 1.4×10^{-6} . The corresponding numbers for the other two strange modes of this model are 2×10^{-6} and 7×10^{-6} . Given the smallness of these numbers, it seems inconceivable that strange modes could threaten the survival of the star on dynamical time-scales.

Whether finite-amplitude strange modes drive mass loss from the shelf is a different and difficult question. On the one hand, the maximum radial velocity at shock onset is rather small ($\lesssim 5$ per cent) compared to the escape velocity $v_{\text{esc}} = (2GM/R)^{1/2}$. On the other hand, the residual between gravitational and radiative accelerations is relatively small, so that escape may be possible at $v \ll v_{\text{esc}}$. Furthermore, line-driven steady winds are likely even without the assistance of shocks. If the mass-loss rate of such a wind is high enough, it may tend to suppress the linear instability of the strange modes. All of this we leave for later investigation.

6 SUMMARY AND DISCUSSION

We have re-examined the stability of the fundamental radial mode of very massive main-sequence stars. Although non-radial and higher order radial modes may also be unstable, we focus on the radial fundamental because collapse or explosion of these radiation-pressure-dominated objects would begin with this mode at linear order. In agreement with SQA, we find that the linear growth rate is sensitive to turbulent convective damping. We have extended their results to higher masses at solar metallicity, and we have used a fully non-adiabatic rather than quasi-adiabatic method, which allows us to treat the κ -mechanism more reliably. The ϵ -mechanism is more important for our most massive models we consider, however.

⁵ Uniform rotation at the mass-shedding limit may set a lower limit to ω_f/ω_* because rotational energy behaves somewhat like gas pressure in the time-dependent virial theorem. Because of the central concentration of $n = 3$ polytropes, however, we estimate that this limit comes into effect only for $M \gtrsim 10^3 M_\odot$, where relativistic corrections must also be considered (Baumgarte & Shapiro 1999).

The linear growth rates remain uncertain not only because of the turbulent bulk viscosity, but also because of the tenuous (and possibly unphysical) envelopes possessed by all of our models above $100 M_\odot$. In fact we find negative growth rates even without convection, apparently due to radiative damping in the shelf. Nevertheless, the growth rate should in any case be extremely small even if positive, $\omega_i/\omega_r \sim \Pi_0/t_{\text{KH}}$, due to the relatively low central concentrations of these stars and correspondingly large mode masses.

We have then argued from the smallness of the linear growth rate (in case this is positive) that the radial fundamental should saturate at a small amplitude due to any one of a number of weak non-linearities. To support this claim, we have estimated the saturation amplitude that would result if parametric coupling to high-order g-modes were the most important non-linearity. For our most massive model, the estimate is $\delta R/R \approx 3 \times 10^{-3}$. Other non-linear couplings may stop the growth at even smaller amplitudes, but those we identify would depend on uncertain parameters such as the star's rotation rate or magnetic field.

We have also shown that our models, like those of GK93, are subject to a class of intrinsically non-adiabatic modes having much larger growth rates but confined to the shelf: strange modes. These we estimate to saturate at fractional surface displacements of a few per cent via shocks. Their contribution to mass loss, if any, can be reliably estimated only in the context of a time-dependent wind model that includes a number of other non-linear effects, such as line driving. However, even at saturation, the energy of the strange modes in the stellar core is negligible, and therefore they probably affect the bulk of the star only secularly.

A number of physical simplifications and compromises have been made: restriction to solar metallicity; neglect of rotation; and neglect of perturbations to the convective flux. Increased metallicity might produce even more extended ‘shelves’ in the equilibrium models, and larger growth rates for the modes driven by the ϵ -mechanism. However, presuming that the growth rates of the fundamental mode varied roughly linearly with Z , they would remain very small compared to the dynamical time even at metallicities 10 times solar, such as may obtain in AGN discs (Dietrich et al. 2003; Nagao, Marconi & Maiolino 2006). Rotation is expected to have a stabilizing influence on the fundamental mode at very high masses because it contributes to the perturbed energy under homologous changes in radius somewhat like gas rather than radiation pressure (Baumgarte & Shapiro 1999). This could be important for very massive stars formed in an AGN disc, and perhaps continually accreting from that disc, since such objects would probably rotate rapidly (Goodman & Tan 2004; Jiang & Goodman 2011). Neglect of perturbations to the convective flux has surely caused quantitative errors in the growth rates. Guzik & Lovekin (2012), using a prescription for such perturbations that incorporates a time delay in the convective response, find that super-Eddington luminosities can occur during part of the pulsation cycle, perhaps leading to mass loss. However, their analysis is limited to the outer parts of the star. More importantly, their prescription relies on mixing-length theory, which may not be reliable in the extremely radiation-pressure-dominated shelf regions (Jiang et al. 2015).

Despite these simplifications and uncertainties, it seems likely that the growth rate of the fundamental mode must be extremely small compared to the reciprocal of the dynamical time, and therefore that pulsations in the fundamental will saturate non-linearly at small amplitudes too small to disrupt or collapse the star – at least on the main sequence. We conclude that thermally driven pulsations of the radial fundamental mode do not limit the main-sequence lifetimes of very massive stars. The tenuous outer envelopes of the more

massive MESA models, however, which stem from an opacity bump at $\sim 10^5$ K, lead us to suspect that these stars would have powerful winds if the hydrostatic constraint were lifted, and that the mass-loss time-scale (\dot{M}_*/\dot{M}) may be much less than 1 Myr, though necessarily longer than the Kelvin–Helmholtz time-scale (≈ 3000 yr). The lower bound would be achieved only if all of the stellar luminosity were converted to the mechanical energy of a wind with vanishing asymptotic velocity at infinity. For a very massive star embedded in a dense AGN disc, continued accretion from the disc might easily exceed the wind losses, perhaps causing it to grow to such a mass as to undergo relativistic instability.

These results suggest a few directions for future research. It will be relatively straightforward to explore the effect of super-solar metallicities on the linear growth rates. Changes in the growth rates as the models evolve away from the ZAMS could also be studied, although we have not yet succeeded in evolving our most massive MESA models to the end of their main-sequence phases. Probably more important, but also more challenging, will be to determine the mass-loss time-scale. Several physical mechanisms will have to be considered, including line-driven winds (Castor, Abbott & Klein 1975); inhomogeneous optically thick winds (Owocki 2015); and perhaps winds driven by non-linear strange modes or other radiation-driven instabilities. Still more mechanisms may operate in late stages of stellar evolution, such as wave-driven winds (Quataert et al. 2015). The range of possibilities is narrowed if one focuses on mechanisms that operate early in the life of a star and that are capable of removing much of its initial mass in much less than the nominal main-sequence lifetime. Even so, multidimensional calculations with frequency-dependent radiative transfer may be required.

ACKNOWLEDGEMENTS

This project made extensive use of the MESA stellar evolution code and the ADIPLS asteroseismology package.

REFERENCES

- Appenzeller I., 1970, *A&A*, 9, 216
 Arras P., Flanagan E. E., Morsink S. M., Schenk A. K., Teukolsky S. A., Wasserman I., 2003, *ApJ*, 591, 1129
 Baumgarte T. W., Shapiro S. L., 1999, *ApJ*, 526, 941
 Benielli D., Sommeria J., 1998, *J. Fluid Mech.*, 374, 117
 Bonanos A. Z. et al., 2004, *ApJ*, 611, L33
 Bono G., Marconi M., Stellingwerf R. F., 1999, *ApJS*, 122, 167
 Brickhill A. J., 1991, *MNRAS*, 251, 673
 Castor J. I., 1971, *ApJ*, 166, 109
 Castor J. I., Abbott D. C., Klein R. I., 1975, *ApJ*, 195, 157
 Chandrasekhar S., 1964, *ApJ*, 140, 417
 Christensen-Dalsgaard J., 2008, *Ap&SS*, 316, 113
 Christy R. F., 1966, *ApJ*, 144, 108
 Cox J. P., 1980, *Theory of Stellar Pulsation*. Princeton Univ. Press, Princeton, NJ
 Cox J. P., Giuli R. T., 1968, *Principles of Stellar Structure*. Gordon & Breach, New York
 Crowther P. A., Schnurr O., Hirschi R., Yusof N., Parker R. J., Goodwin S. P., Kassim H. A., 2010, *MNRAS*, 408, 731
 Davey A., 1983, *J. Comput. Phys.*, 51, 343
 Dhanda Batra N., Baldwin J. A., 2014, *MNRAS*, 439, 771
 Dietrich M., Hamann F., Shields J. C., Constantin A., Heidt J., Jäger K., Vestergaard M., Wagner S. J., 2003, *ApJ*, 589, 722
 Drury L. O., 1980, *J. Comput. Phys.*, 37, 133
 Dziembowski W., 1982, *Acta Astron.*, 32, 147
 Figier D. F., 2005, *Nature*, 434, 192
 Glatzel W., Kiriakidis M., 1993, *MNRAS*, 262, 85 (GK93)
 Goodman J., Tan J. C., 2004, *ApJ*, 608, 108
 Gräfener G., Owocki S. P., Vink J. S., 2012, *A&A*, 538, A40
 Grevesse N., Noels A., 1993, *Phys. Scr. T*, T47, 133
 Guzik J. A., Lovekin C. C., 2012, *Astron. Rev.*, 7, 13
 Hamann F., Ferland G., 1999, *ARA&A*, 37, 487
 Henyey L., Vardya M. S., Bodenheimer P., 1965, *ApJ*, 142, 841
 Hurley M., Roberts P. H., 1964, *ApJ*, 140, 583
 Iglesias C. A., Rogers F. J., 1996, *ApJ*, 464, 943
 Jiang Y.-F., Goodman J., 2011, *ApJ*, 730, 45
 Jiang Y.-F., Cantiello M., Bildsten L., Quataert E., Blaes O., 2015, *ApJ*, 813, 74
 Koen C., 2006, *MNRAS*, 365, 590
 Kumar P., Goldreich P., 1989, *ApJ*, 342, 558
 Matsuoka K., Nagao T., Marconi A., Maiolino R., Taniguchi Y., 2011, *A&A*, 527, A100
 Montero P. J., Janka H.-T., Müller E., 2012, *ApJ*, 749, 37
 Nagao T., Marconi A., Maiolino R., 2006, *A&A*, 447, 157
 Oey M. S., Clarke C. J., 2005, *ApJ*, 620, L43
 Owocki S. P., 2015, in Vink J. S., ed., *Astrophysics and Space Science Library*, Vol. 412, *Very Massive Stars in the Local Universe*. Springer-Verlag, Switzerland, p. 113
 Papaloizou J. C. B., 1973a, *MNRAS*, 162, 143
 Papaloizou J. C. B., 1973b, *MNRAS*, 162, 169
 Papaloizou J. C. B., Alberts F., Pringle J. E., Savonije G. J., 1997, *MNRAS*, 284, 821
 Paxton B., Bildsten L., Dotter A., Herwig F., Lesaffre P., Timmes F., 2011, *ApJS*, 192, 3
 Paxton B. et al., 2013, *ApJS*, 208, 4
 Quataert E., Fernandez R., Kasen D., Klion H., Paxton B., 2015, preprint ([arXiv e-prints](https://arxiv.org/abs/1508.01513))
 Rauw G. et al., 2004, *A&A*, 420, L9
 Schenk A. K., Arras P., Flanagan E. E., Teukolsky S. A., Wasserman I., 2002, *Phys. Rev. D*, 65, 024001
 Schnurr O., 2012, in Drissen L., Rubert C., St-Louis N., Moffat A. F. J., eds, *ASP Conf. Ser. Vol. 465, Proceedings of a Scientific Meeting in Honor of Anthony F. J. Moffat*. Astron. Soc. Pac., San Francisco, p. 187
 Schwarzschild M., Härm R., 1959, *ApJ*, 129, 637
 Shiode J. H., Quataert E., Arras P., 2012, *MNRAS*, 423, 3397 (SQA)
 Weidner C., Kroupa P., 2004, *MNRAS*, 348, 187
 Wu Y., Goldreich P., 2001, *ApJ*, 546, 469
 Zeldovich Y. B., Novikov I. D., 1971, *Relativistic Astrophysics*. Vol. 1, *Stars and Relativity*. University of Chicago Press, Chicago

APPENDIX A: METHOD FOR STIFF LINEAR BOUNDARY-VALUE PROBLEMS

The method described here is similar to that of Drury (1980) and Davey (1983), but different in detail and slightly simpler, at least in derivation. One wants to solve

$$\frac{dy}{dx} = \mathbf{A}y, \quad (\text{A1})$$

\mathbf{y} being a column vector of length n representing the dependent variables, and \mathbf{A} an $n \times n$ matrix depending upon an eigenvalue to be determined, and usually also on the independent variable, x . In our case $n = 4$, and the eigenvalue is the complex frequency of pulsation, ω . There are p homogeneous boundary conditions to be satisfied at the left-hand boundary, $x = x_{\min}$, and $n - p$ at the right-hand boundary, $x = x_{\max}$. These are represented by $p \times n$ and $(n - p) \times n$ matrices $\mathbf{B}(x_{\min})$ and $\mathbf{C}(x_{\max})$:

$$\mathbf{B}(x_{\min})\mathbf{y}(x_{\min}) = 0, \quad \mathbf{C}(x_{\max})\mathbf{y}(x_{\max}) = 0. \quad (\text{A2})$$

One expects non-zero solutions for $\mathbf{y}(x)$ only for discrete values of ω , which are to be determined.

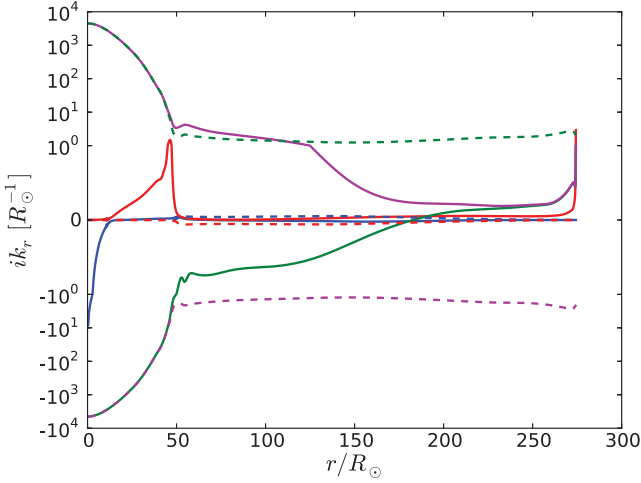


Figure A1. Real (solid) and imaginary (dashed) parts of the four eigenvalues of \mathbf{A} in the 938 M_{\odot} model. Vertical scale is linear within the interval $(-R_{\odot}^{-1}, R_{\odot}^{-1})$, and logarithmic outside it.

The difficulty in solving this boundary-value problem is that the n complex eigenvalues of $\mathbf{A}(x, \omega)$ may differ widely in size (Fig. A1). In our problem, they vary over 4–6 orders of magnitude in the inner parts of the star, due to the large ratio of thermal to dynamical time.⁶ Furthermore, since the eigenfunction corresponding to λ behaves as $\sim \exp(\int^x \lambda dx)$, direct integration of equation (A1) can overflow or underflow machine precision if the real part of λ is large. This happens in our stellar problem, and both signs of $\text{Real}(\lambda)$ occur simultaneously. It therefore proves impractical to use a conventional shooting method in which one iteratively makes guesses for the unconstrained components of \mathbf{y} at both boundaries (and for ω) and integrates towards a fitting point. As described above, a relaxation (Henyei-type) method also failed.

Instead, we propagate the boundary conditions themselves to the fitting point. For a given choice of ω and for any x and x' between the boundaries, equation (A1) has the formal solution $\mathbf{y}(x) = \mathbf{P}(x, x')\mathbf{y}(x')$ if the ‘propagator’ \mathbf{P} satisfies

$$\begin{aligned} \frac{\partial \mathbf{P}}{\partial x}(x, x') &= \mathbf{A}(x)\mathbf{P}(x, x'), & \frac{\partial \mathbf{P}}{\partial x'}(x, x') &= -\mathbf{P}(x, x')\mathbf{A}(x'), \\ \mathbf{P}(x, x') &= \mathbf{P}(x, x'')\mathbf{P}(x'', x'), & \mathbf{P}(x, x) &= \mathbf{I}, \end{aligned} \quad (\text{A3})$$

\mathbf{I} being the $n \times n$ identity. The left-hand boundary condition (A2) can then be restated as $\mathbf{B}(\bar{x})\mathbf{y}(\bar{x}) = 0$ with $\mathbf{B}(\bar{x}) \equiv \mathbf{B}(x_{\min})\mathbf{P}(x_{\min}, \bar{x})$. Similarly $\mathbf{C}(\bar{x})\mathbf{y}(\bar{x}) = 0$ with $\mathbf{C}(\bar{x}) \equiv \mathbf{C}(x_{\max})\mathbf{P}(x_{\max}, \bar{x})$. In other words, the solution $\mathbf{y}(\bar{x})$ at any intermediate \bar{x} between x_{\min} and x_{\max} must belong to the subspace annihilated by $\mathbf{B}(\bar{x})$, and also to the subspace annihilated by $\mathbf{C}(\bar{x})$. Since the dimensions of these two subspaces add up to n , their intersection is only $\mathbf{y} = 0$ unless ω is a root of

$$\det\{\mathbf{B}(\bar{x}), \mathbf{C}(\bar{x})\} = 0, \quad (\text{A4})$$

$\{\mathbf{B}, \mathbf{C}\}$ meaning the $n \times n$ matrix whose first p rows coincide with those of \mathbf{B} and whose last $n - p$ rows those of \mathbf{C} .

⁶ The eigenvalues $\{\lambda_1, \dots, \lambda_n\}$ of \mathbf{A} at a particular x should not be confused with the eigenvalue ω of the entire boundary-value problem. It might be better to speak of wavenumbers $k_x \equiv -i\lambda$. Since \mathbf{A} depends upon ω as well as x , the λ s and k_x s do as well.

This reformulation may appear pointless since it is no easier to solve for \mathbf{P} by direct integration of equation (A2) than to solve equation (A1) itself. The same difficulties with stiffness and overflow occur. Furthermore, as the separation between \bar{x} and x_{\min} increases, the rows of $\mathbf{B}(\bar{x})$ are dominated by the fastest growing eigenvector of \mathbf{A} , so that they quickly become linearly dependent when estimated in finite-precision arithmetic. A key observation, however, is that the constraint $\mathbf{B}(x)\mathbf{y}(x) = 0$ is equivalent to $\mathbf{L}\mathbf{B}(x)\mathbf{y}(x) = 0$ for any non-singular $p \times p$ matrix \mathbf{L} . This can be exploited to keep the rows of $\mathbf{L}\mathbf{B}(x)$ linearly independent, in fact orthonormal.

In practice one integrates equation (A1) or equation (A2) on a discrete grid $x_{\min} = x_0 < x_1 < x_2 \dots < x_N = x_{\max}$. Let x_m be the fitting point, $0 < m < N$. The values of $\mathbf{B}(x_k)$ could be defined iteratively according to

$$\mathbf{B}(x_{k+1}) = \mathbf{B}(x_k)\mathbf{P}(x_k, x_{k+1}), \quad \mathbf{B}(x_0) = \mathbf{B}(x_{\min}).$$

Instead of this, however, we solve

$$\hat{\mathbf{B}}_{k+1} = \mathbf{G}_{k+1}\hat{\mathbf{B}}_k\hat{\mathbf{P}}_{k,k+1}, \quad \hat{\mathbf{B}}_0 = \mathbf{B}(x_{\min}). \quad (\text{A5})$$

Here $\hat{\mathbf{P}}_{k,k+1}$ is a discrete approximation to $\mathbf{P}(x_k, x_{k+1})$ – a suitable choice will be given presently – while \mathbf{G}_{k+1} is chosen at each step to make the rows of $\hat{\mathbf{B}}_{k+1}$ orthonormal. For example, if $p = 2$ and the rows of $\hat{\mathbf{B}}_k\hat{\mathbf{P}}_{k,k+1}$ are \mathbf{a} and \mathbf{b} , then

$$\mathbf{G}_{k+1} = \begin{pmatrix} 1 & 0 \\ 0 & \gamma \end{pmatrix} \begin{pmatrix} 1 & 0 \\ -\beta & 1 \end{pmatrix} \begin{pmatrix} \alpha & 0 \\ 0 & 1 \end{pmatrix}, \quad (\text{A6})$$

with $\alpha \equiv |\mathbf{a}|^{-1}$, $\beta \equiv \mathbf{a}\mathbf{b}\mathbf{a}^\dagger$, and $\gamma \equiv |\mathbf{b} - \alpha\beta\mathbf{a}|^{-1}$. This represents the Gram–Schmidt process, which can be extended to any number of rows. It is clear that if $\hat{\mathbf{P}}_{k+1} = \mathbf{P}(x_k, x_{k+1})$, then $\hat{\mathbf{B}}_m = \mathbf{G}_0\mathbf{G}_1 \dots \mathbf{G}_m\mathbf{B}(x_m)$, so that $\det \mathbf{B}(x_m) = 0$ if and only if $\det \hat{\mathbf{B}}_m = 0$.

We now discuss a suitable approximation for $\mathbf{P}(x_k, x_{k+1})$. If \mathbf{A} were constant over the interval $[x_k, x_{k+1}]$, then $\hat{\mathbf{P}}_{k,k+1} = \exp[(x_{k+1} - x_k)\mathbf{A}]$ would be exact, and otherwise if \mathbf{A} is evaluated at the midpoint $x_{k+1/2} \equiv (x_k + x_{k+1})/2$, then the exponential approximation formally second order in $\Delta x_k \equiv x_{k+1} - x_k$. However, in our problem, the largest eigenvalue of $\mathbf{A}_{k+1/2}$ can be so large that on a reasonable mesh (we typically interpolate the MESA model with splines at $\sim 10^3$ – 10^4 uniformly spaced radii), the matrix exponential can overflow, or at least cause substantial loss of precision. We therefore adopt the Crank–Nicholson approximation:

$$\hat{\mathbf{P}}_{k,k+1} = \left(\mathbf{I} + \frac{1}{2}\Delta x_k \mathbf{A}_{k+1/2} \right) \left(\mathbf{I} - \frac{1}{2}\Delta x_k \mathbf{A}_{k+1/2} \right)^{-1}. \quad (\text{A7})$$

Eigenvalues of $\mathbf{A}_{k+1/2}$ with positive (negative) real part, corresponding to behaviours that grow (decay) with increasing x , are mapped to eigenvalues of $\hat{\mathbf{P}}_{k,k+1}$ inside (outside) the unit circle, presuming $x_k < x_{k+1}$; very large eigenvalues of $\Delta x_k \mathbf{A}_{k+1/2}$ are mapped to eigenvalues of $\hat{\mathbf{P}}_{k,k+1}$ close to -1 . It is still necessary to use a mesh fine enough so that the behaviours that should decay with the iteration (A5) do so quickly enough; the growing behaviours are controlled by the orthonormalization. In practice this is determined by varying the mesh resolution and monitoring the effect on the estimated root of equation (A4) for ω .

Another constraint on the mesh is that the Crank–Nicholson approximation (A7) for $\mathbf{P}(x_k, x_{k+1})$ encounters a pole if $\mathbf{A}_{k+1/2}$ has $2/\Delta x_k$ as an eigenvalue. In fact, the eigenvalue represented by the blue lines in Fig. A1 is nearly real and diverges towards the centre of the star. This corresponds approximately to the singular solution of the adiabatic equation, $\propto r^{-3}$ as $r \rightarrow 0$. To control this, we start the integration at a non-zero but small radius r_{\min} with a mesh spacing $\Delta r \ll r_{\min}/3$. This ensures that no poles are

encountered as we integrate outward, since the other two large eigenvalues, which represent strongly non-adiabatic heat diffusion, have almost equal real and imaginary parts,⁷ so that they cannot cause poles for real values of $\Delta x_k = \Delta r$.

The right-hand boundary condition is translated to the matching point by constructing the $(n - p) \times p$ matrix $\hat{\mathbf{C}}_m$ in similar fashion.

A1 Analyticity

In many problems of physical interest, the components of the matrix \mathbf{A} depend analytically or even polynomially on the eigenvalue ω . Such is the case in our stellar problem, since ω is a temporal frequency and there are a finite number of time derivatives in the linearized equations. The matrices $\mathbf{P}(x, x')$, $\mathbf{B}(x)$, $\mathbf{C}(x)$, and the determinant (A4) can then be expected also to depend analytically on ω , i.e. their derivatives with respect to ω satisfy the Cauchy–Riemann equations. It is desirable to have a numerical scheme that preserves this analyticity up to round-off error, notwithstanding truncation error. For one thing, if $F(\omega)$ represents the determinant (A4), then the roots of $F(\omega) = 0$ can be sought by an efficient algorithm that assumes analyticity. The simplest of these, and what we use, is false position,

$$\hat{\omega}_{n+1} = \frac{\hat{\omega}_{n-1}\hat{F}(\hat{\omega}_n) - \hat{\omega}_n\hat{F}(\hat{\omega}_{n-1})}{\hat{F}(\hat{\omega}_n) - \hat{F}(\hat{\omega}_{n-1})}. \quad (\text{A8})$$

This is only a minor convenience since the root could be sought by treating the real and imaginary parts of $\hat{\omega}$ (and of \hat{F}) as independent. More importantly, the convergence of equation (A8) for complex $\hat{\omega}$ depends upon the extent to which

⁷ They satisfy $-i\omega\delta T \approx \eta\partial^2\delta T/\partial r^2$, where $\eta = 16\sigma_{\text{SB}}T^3/3\kappa\rho^2c_p$ is the thermal diffusivity. Hence the eigenvalues $ik_r \approx \pm\sqrt{-i\omega/\eta}$.

$$\frac{\hat{F}(\omega + i\epsilon) - \hat{F}(\omega)}{i\epsilon} \approx \frac{\hat{F}(\omega + \epsilon) - \hat{F}(\omega)}{\epsilon}, \quad |\epsilon| \ll |\omega|, \quad (\text{A9})$$

and so can be used to monitor the effects of round-off error.

The numerical scheme described above is *not* analytic in ω , even in exact arithmetic, because of the complex conjugations involved in the orthonormalization matrices \mathbf{G}_k and \mathbf{L} . That is to say, if $\hat{F}(\omega)$ were defined as the determinant that results from replacing $\mathbf{B}(\bar{x})$ and $\mathbf{C}(\bar{x})$ with $\hat{\mathbf{B}}_m$ and $\hat{\mathbf{C}}_m$ in equation (A4), then it would not be analytic in ω . However, analyticity can be rescued by the following simple trick. The condition $\hat{\mathbf{B}}_m \mathbf{y}_m = 0$ constitutes p constraints on the n components of \mathbf{y}_m . Therefore, it can be rewritten as

$$\mathbf{v} = \tilde{\mathbf{B}}\mathbf{u}, \quad (\text{A10})$$

where \mathbf{u} is a column vector containing the first $n - p$ components of \mathbf{y}_m , \mathbf{v} contains the remaining p components, and $\tilde{\mathbf{B}}$ is $p \times (n - p)$. Now it is easy to see that $\tilde{\mathbf{B}}$ is independent of the non-analytic orthonormalizing factors $\mathbf{G}_0 \cdots \mathbf{G}_N \equiv \mathbf{L}$ defined via equations (A5) and (A6), at least in principle, since $\hat{\mathbf{B}}_m \mathbf{y}_m = 0$ is equivalent to $\mathbf{L}^{-1}\hat{\mathbf{B}}_m \mathbf{y}_m = 0$, and the latter is analytic. Similarly, we can rewrite the translated right-hand boundary condition $\hat{\mathbf{C}}_m \mathbf{y}_m = 0$ as $\mathbf{u} = \tilde{\mathbf{C}}\mathbf{v}$. Eliminating \mathbf{u} between this and equation (A10) leads to

$$\hat{F}(\omega) \equiv \det(\tilde{\mathbf{B}}\tilde{\mathbf{C}} - \mathbf{I}) = 0. \quad (\text{A11})$$

This is analytic, apart from roundoff error, as we have confirmed numerically via equation (A9) and by the convergence of the iteration (A8) to the level $|\Delta\omega/\omega| \lesssim 10^{-9}$.

This paper has been typeset from a $\text{\TeX}/\text{\LaTeX}$ file prepared by the author.